Perspectives of seismic imaging using FWI with reciprocity misfit functional

Florian Faucher

To cite this version:

Florian Faucher. Perspectives of seismic imaging using FWI with reciprocity misfit functional. Journées Ondes Sud-Ouest (JOSO), Mar 2019, Le Barp, France. hal-02076212

HAL Id: hal-02076212
https://hal.archives-ouvertes.fr/hal-02076212

Submitted on 22 Mar 2019

HAL is a multi-disciplinary open access archive for the deposit and dissemination of scientific research documents, whether they are published or not. The documents may come from teaching and research institutions in France or abroad, or from public or private research centers.

L'archive ouverte pluridisciplinaire **HAL**, est destinée au dépôt et à la diffusion de documents scientifiques de niveau recherche, publiés ou non, émanant des établissements d'enseignement et de recherche français ou étrangers, des laboratoires publics ou privés.

Perspectives of seismic imaging using FWI with reciprocity misfit functional

Florian Faucher[1],

Giovanni Alessandrini[2], Hélène Barucq[1], Maarten V. de Hoop[3], Romina Gaburro[4] and Eva Sincich[2].

Journées Ondes Sud-Ouest, CEA Cesta, France

Marth 12th–14th, 2019

[1] Project-Team Magique-3D, Inria Bordeaux Sud-Ouest, France.

[2] Dipartimento di Matematica e Geoscienze, Università di Trieste, Italy.

[3] Department of Computational and Applied Mathematics and Earth Science, Rice University, Houston, USA

[4] Department of Mathematics and Statistics, Health Research Institute (HRI), University of Limerick, Ireland.

Overview

Plan

1. Introduction

Seismic inverse problem

Reconstruction of subsurface Earth properties from seismic campaign: collection of **wave** propagation data at the surface.

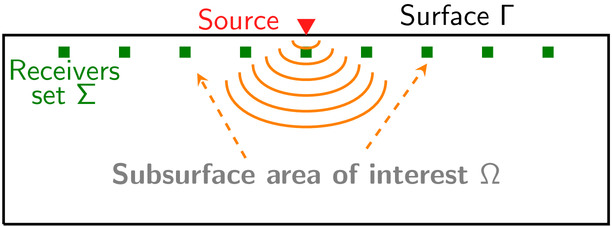

Seismic data

We work with back-scattered partial data from one-side illumination on large domain.

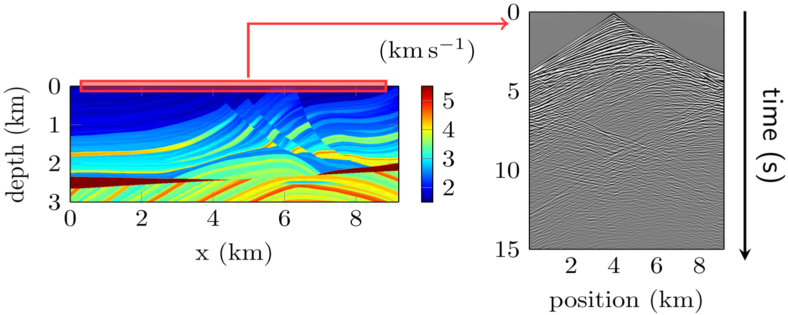

Seismic data

We work with back-scattered partial data from one-side illumination on large domain.

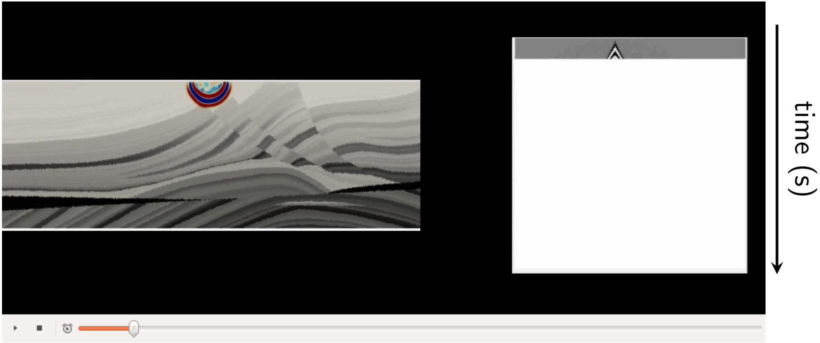

Seismic data

We work with back-scattered partial data from one-side illumination on large domain.

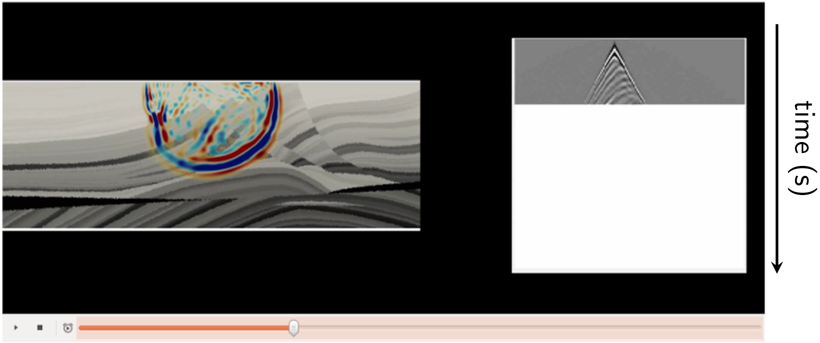

Seismic data

We work with back-scattered partial data from one-side illumination on large domain.

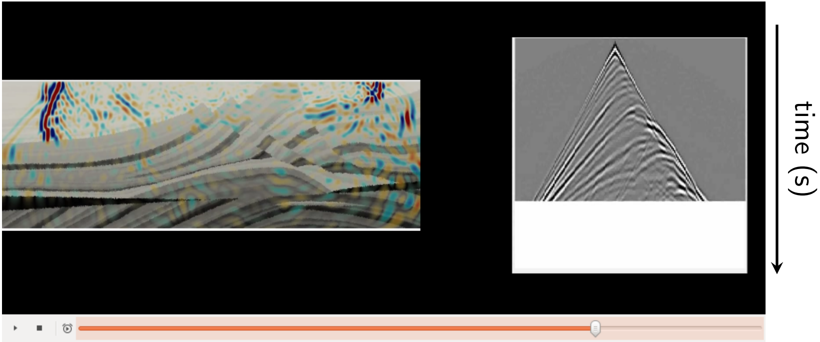

Seismic data

Inverse problem: from seismic traces to subsurface?

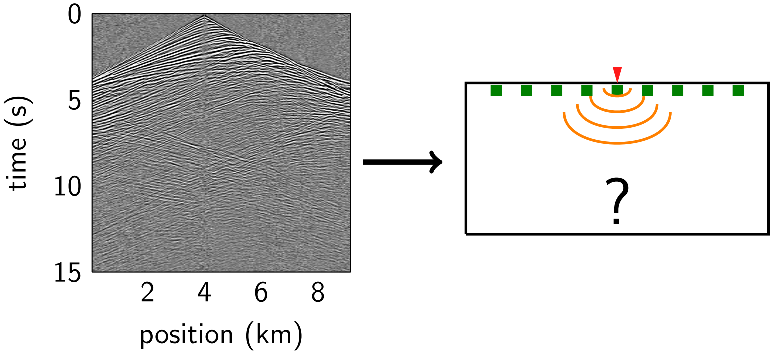

nonlinear, ill-posed inverse problem.

Plan

2. Time-Harmonic Inverse Problem, FWI

Time-harmonic wave equation

We consider propagation in acoustic media, given by the Euler's equations, heterogeneous medium parameters κ and ρ:

$$\begin{cases} -\mathrm{i}\omega\rho(\boldsymbol{x})\boldsymbol{v}(\boldsymbol{x}) = -\nabla p(\boldsymbol{x}), \\ -\mathrm{i}\omega p(\boldsymbol{x}) = -\kappa(\boldsymbol{x})\nabla \cdot \boldsymbol{v}(\boldsymbol{x}) + f(\boldsymbol{x}). \end{cases}$$

p: scalar pressure field,
$\boldsymbol{v}$: vectorial velocity field,
f: source term,

κ: bulk modulus,
ρ: density,
ω: angular frequency.

Time-harmonic wave equation

We consider propagation in acoustic media, given by the Euler's equations, heterogeneous medium parameters κ and ρ:

$$\begin{cases} -\mathrm{i}\omega\rho(\boldsymbol{x})\boldsymbol{v}(\boldsymbol{x}) = -\nabla p(\boldsymbol{x}), \\ -\mathrm{i}\omega p(\boldsymbol{x}) = -\kappa(\boldsymbol{x})\nabla\cdot\boldsymbol{v}(\boldsymbol{x}) + f(\boldsymbol{x}). \end{cases}$$

p: scalar pressure field,	κ: bulk modulus,
$\boldsymbol{v}$: vectorial velocity field,	ρ: density,
f: source term,	ω: angular frequency.

The system reduces to the Helmholtz equation when ρ is constant,

$$(-\omega^2 c(\boldsymbol{x})^{-2} - \Delta)p(\boldsymbol{x}) = 0,$$

$$\text{with} \quad c(\boldsymbol{x}) = \sqrt{\kappa(\boldsymbol{x})\rho(\boldsymbol{x})^{-1}}.$$

Dual-sensors devices

The inverse problem aims the recovery of the subsurface medium parameters from surface measurements of pressure **and** normal (vertical) velocity:

$$\mathcal{F} : m = (\kappa, \rho) \quad \rightarrow \quad \{\mathcal{F}_p \; ; \; \mathcal{F}_v\} = \Big\{p(\boldsymbol{x}_1), p(\boldsymbol{x}_2), \ldots, p(\boldsymbol{x}_{n_{rcv}}); \\ v_n(\boldsymbol{x}_1), v_n(\boldsymbol{x}_2), \ldots, v_n(\boldsymbol{x}_{n_{rcv}})\Big\}.$$

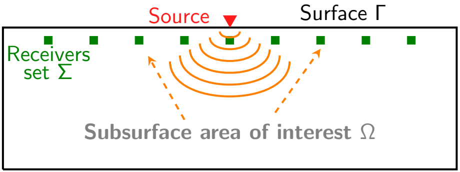

D. Carlson, N. D. Whitmore *et al.*
Increased resolution of seismic data from a dual-sensor streamer cable – Imaging of primaries and multiples using a dual-sensor towed streamer
SEG, 2007 – 2010

CGG & Lundun Norway (2017–2018)
TopSeis acquisition (`www.cgg.com/en/What-We-Do/Offshore/Products-and-Solutions/TopSeis`)

Full Waveform Inversion (FWI)

FWI provides a **quantitative reconstruction** of the subsurface parameters by solving a minimization problem,

$$\min_{m \in \mathcal{M}} \quad \mathcal{J}(m) = \frac{1}{2} \|\mathcal{F}(m) - d\|^2.$$

- d are the observed data,
- $\mathcal{F}(m)$ represents the simulation using an initial model m:

P. Lailly
The seismic inverse problem as a sequence of before stack migrations
Conference on Inverse Scattering: Theory and Application, SIAM, 1983

A. Tarantola
Inversion of seismic reflection data in the acoustic approximation
Geophysics, 1984

A. Tarantola
Inversion of travel times and seismic waveforms
Seismic tomography, 1987

FWI, iterative minimization

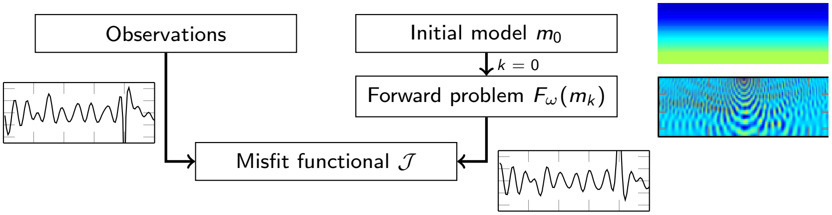

FWI, iterative minimization

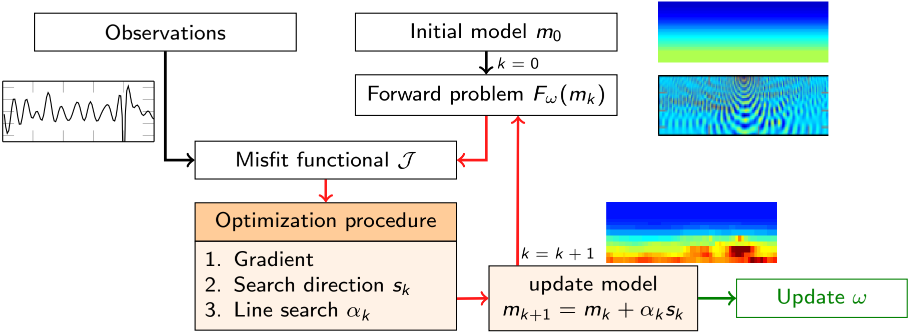

FWI, iterative minimization

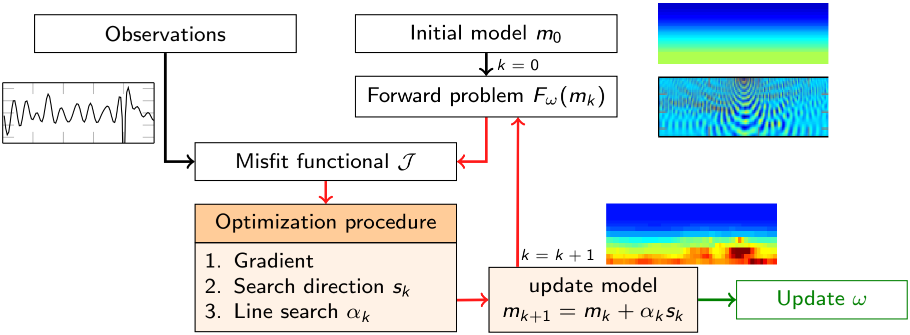

Numerical methods

- Adjoint-method for the gradient computation, L-BFGS method,
- forward problem resolution with Discontinuous Galerkin methods,
- parallel computation, HPC, large-scale optimization,
- Rk: the code also works for elastic anisotropy and viscous media.

FWI, iterative minimization

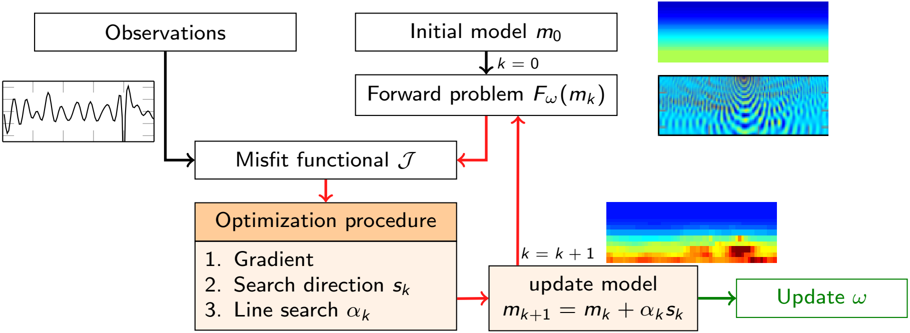

- $> 10^5$: unknowns per physical parameter,
- $> 10^6$: matrix size for discretization,
- we also study stability and convergence of the algorithm ...

Plan

3 Reconstruction procedure using dual-sensors data

Minimization of the cost function

The appropriate misfit functional to minimize with pressure and vertical velocity measurements.

- Compare the pressure and velocity fields separately:

$$\mathcal{J}_{L2} = \sum_{source} \frac{1}{2}\|\mathcal{F}_p^{(s)} - d_p^{(s)}\|^2 + \frac{1}{2}\|\mathcal{F}_v^{(s)} - d_v^{(s)}\|^2.$$

Minimization of the cost function

The appropriate misfit functional to minimize with pressure and vertical velocity measurements.

- Compare the pressure and velocity fields separately:

$$\mathcal{J}_{L2} = \sum_{source} \frac{1}{2} \| \mathcal{F}_p^{(s)} - d_p^{(s)} \|^2 + \frac{1}{2} \| \mathcal{F}_v^{(s)} - d_v^{(s)} \|^2 .$$

- Compare the fields multiplication for all combinations:

$$\mathcal{J}_{\mathcal{G}} = \frac{1}{2} \sum_{s_1} \sum_{s_2} \| d_v^{(s_1)\,T} \mathcal{F}_p^{(s_2)} - d_p^{(s_1)\,T} \mathcal{F}_v^{(s_2)} \|^2 .$$

G. Alessandrini, M.V. de Hoop, F. F., R. Gaburro and E. Sincich
Inverse problem for the Helmholtz equation with Cauchy data: reconstruction with conditional well-posedness driven iterative regularization
preprint

Minimization of the cost function

$$\mathcal{J}_{\mathcal{G}} = \frac{1}{2} \sum_{s_1} \sum_{s_2} \| d_v^{(s_1)\,T} \mathcal{F}_p^{(s_2)} - d_p^{(s_1)\,T} \mathcal{F}_v^{(s_2)} \|^2.$$

From Euler's equation, $v_n(\boldsymbol{x}_i) = -\mathrm{i}(\omega\rho)^{-1}\partial_n p(\boldsymbol{x}_i)$.

Minimization of the cost function

$$\mathcal{J}_{\mathcal{G}} = \frac{1}{2} \sum_{s_1} \sum_{s_2} \| d_v^{(s_1)\,T} \mathcal{F}_p^{(s_2)} - d_p^{(s_1)\,T} \mathcal{F}_v^{(s_2)} \|^2.$$

From Euler's equation, $v_n(\boldsymbol{x}_i) = -\mathrm{i}(\omega\rho)^{-1}\partial_n p(\boldsymbol{x}_i)$.

- **Cauchy data**: the cost function follows **Green's identity**.

Minimization of the cost function

$$\mathcal{J}_{\mathcal{G}} = \frac{1}{2} \sum_{s_1} \sum_{s_2} \| d_v^{(s_1)\,T} \mathcal{F}_p^{(s_2)} - d_p^{(s_1)\,T} \mathcal{F}_v^{(s_2)} \|^2 .$$

From Euler's equation, $v_n(\boldsymbol{x}_i) = -\mathrm{i}(\omega\rho)^{-1}\partial_n p(\boldsymbol{x}_i)$.

- **Cauchy data**: the cost function follows **Green's identity**.
- **Reciprocity gap functional** in inverse scattering.

D. Colton and H. Haddar
An application of the reciprocity gap functional to inverse scattering theory
Inverse Problems 21 (1) (2005), 383398.

G. Alessandrini, M.V. de Hoop, R. Gaburro and E. Sincich
Lipschitz stability for a piecewise linear Schrödinger potential from local Cauchy data
arXiv:1702.04222, 2017

G. Alessandrini, M.V. de Hoop, F. F., R. Gaburro and E. Sincich
Inverse problem for the Helmholtz equation with Cauchy data: reconstruction with conditional well-posedness driven iterative regularization
preprint

Stability results

Lipschitz type stability is obtained for the Helmholtz equation with **partial Cauchy data**.

$$\|c_1 - c_2\| \leq \mathcal{C}\big(\mathcal{J}_{\mathcal{G}}(c_1, c_2)\big)^{1/2}$$

Stability results

Lipschitz type stability is obtained for the Helmholtz equation with **partial Cauchy data**.

$$\|c_1 - c_2\| \leq \mathcal{C}\left(\mathcal{J}_{\mathcal{G}}(c_1, c_2)\right)^{1/2}$$

- Using back-scattered data from one side in a domain with free surface and absorbing conditions,

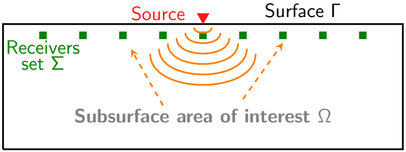

- for piecewise linear parameters.

G. Alessandrini, M.V. de Hoop, R. Gaburro and E. Sincich
Lipschitz stability for a piecewise linear Schrödinger potential from local Cauchy data
arXiv:1702.04222, 2017

G. Alessandrini, M.V. de Hoop, F. F., R. Gaburro and E. Sincich
Inverse problem for the Helmholtz equation with Cauchy data: reconstruction with conditional well-posedness driven iterative regularization

Additional possibilities

It allows the non-collocation of numerical and observational sources:

$$\mathcal{J}_{\mathcal{G}} = \frac{1}{2} \sum_{s_1} \sum_{s_2} \| d_v^{(s_1)\,T} \mathcal{F}_p^{(s_2)} - d_p^{(s_1)\,T} \mathcal{F}_v^{(s_2)} \|^2 .$$

- s_1 is fixed by the observational setup,
- s_2 is chosen for the numerical comparisons.

Plan

4 Numerical experiments

- Comparison of misfit functions
- Changing the numerical acquisition with $\mathcal{J}_{\mathcal{G}}$

Experiment setup

3D velocity model $2.5 \times 1.5 \times 1.2$km using dual-sensors data.

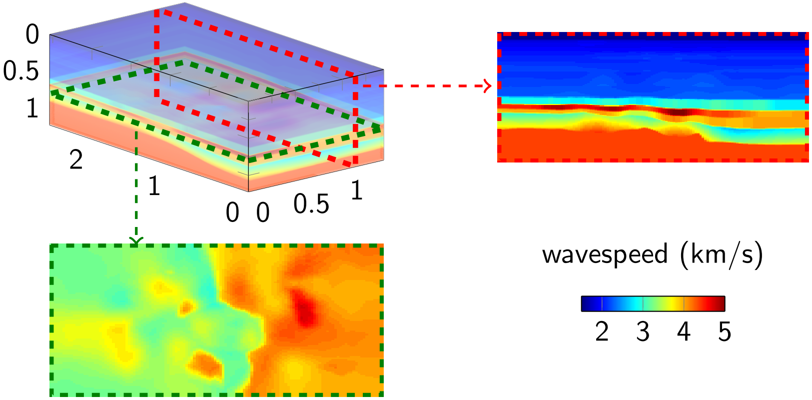

Experiment setup

We work with time-domain data acquisition.

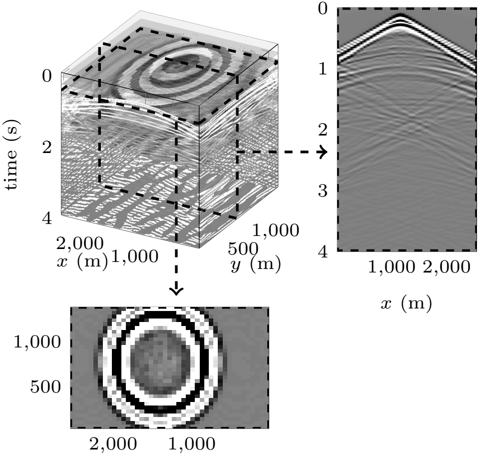

Experiment setup

We work with time-domain data (pressure and velocity).

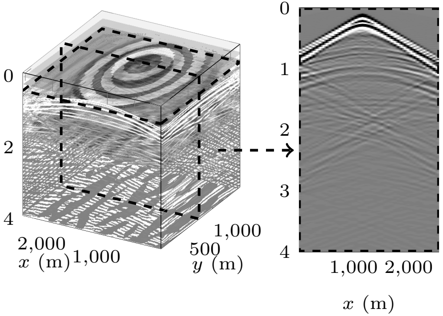

Acquisition for the measures

- 160 sources,
- 100 m depth,
- point source,

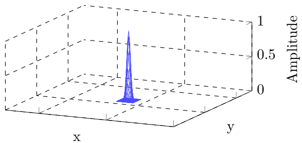

For the reconstruction, we apply a Fourier transform of the time data.

Comparison of misfit functional

We respect the observational acquisition setup and perform the minimization of $\mathcal{J}_{L2}$ or $\mathcal{J}_{\mathcal{G}}$, frequency from 3 to 15Hz.

$$\mathcal{J}_{L2} = \sum_{source} \frac{1}{2} \| \mathcal{F}_p^{(s)} - d_p^{(s)} \|^2 + \frac{1}{2} \| \mathcal{F}_v^{(s)} - d_v^{(s)} \|^2 .$$

$$\mathcal{J}_{\mathcal{G}} = \frac{1}{2} \sum_{source} \sum_{source} \| d_v^{(s_1)\,T} \mathcal{F}_p^{(s_2)} - d_p^{(s_1)\,T} \mathcal{F}_v^{(s_2)} \|^2 .$$

Comparison of misfit functional

We respect the observational acquisition setup and perform the minimization of $\mathcal{J}_{L2}$ or $\mathcal{J}_{\mathcal{G}}$, frequency from 3 to 15Hz.

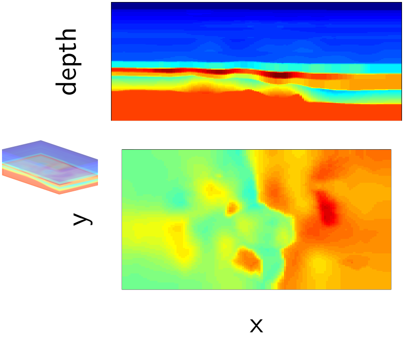

(a) True velocity

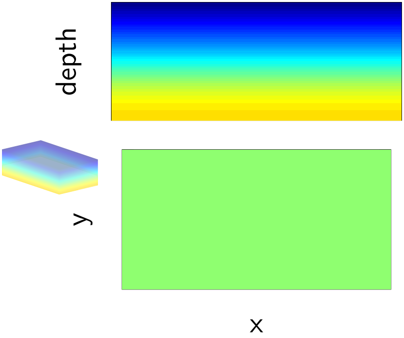

(b) Starting velocity

Comparison of misfit functional

We respect the observational acquisition setup and perform the minimization of $\mathcal{J}_{L2}$ or $\mathcal{J}_{\mathcal{G}}$, frequency from 3 to 15Hz.

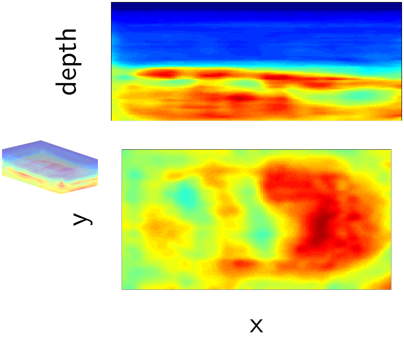

(a) Using $\mathcal{J}_{L2}$

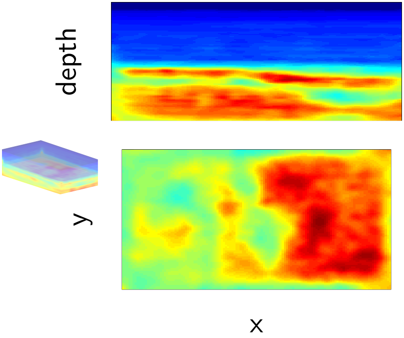

(b) Using $\mathcal{J}_{\mathcal{G}}$

Comparison of misfit functional

We respect the observational acquisition setup and perform the minimization of $\mathcal{J}_{L2}$ or $\mathcal{J}_{\mathcal{G}}$, frequency from 3 to 15Hz.

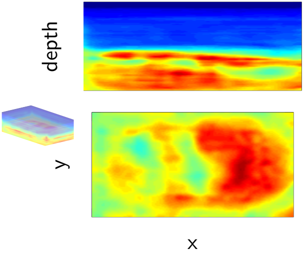

(a) Using $\mathcal{J}_{L2}$

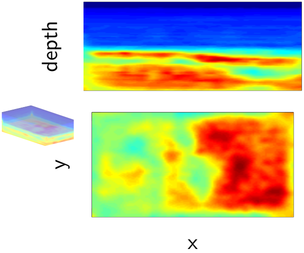

(b) Using $\mathcal{J}_{\mathcal{G}}$

But the major advantage of $\mathcal{J}_{\mathcal{G}}$ is the possibility to consider alternative acquisition setup.

Experiment with different obs. and sim. acquisition

$$\min \mathcal{J}_{\mathcal{G}} = \frac{1}{2} \sum_{s_1} \sum_{s_2} \| d_v^{(s_1)\,T} \mathcal{F}_p^{(s_2)} - d_p^{(s_1)\,T} \mathcal{F}_v^{(s_2)} \|^2.$$

Acquisition for the measures s_1

- 160 sources,
- 100 m depth,
- point source,

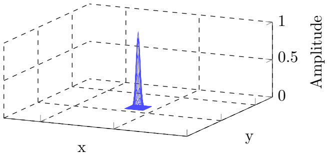

Experiment with different obs. and sim. acquisition

$$\min \mathcal{J}_{\mathcal{G}} = \frac{1}{2} \sum_{s_1} \sum_{s_2} \| d_v^{(s_1)\,T} \mathcal{F}_p^{(s_2)} - d_p^{(s_1)\,T} \mathcal{F}_v^{(s_2)} \|^2.$$

Acquisition for the measures s_1

- 160 sources,
- 100 m depth,
- point source,

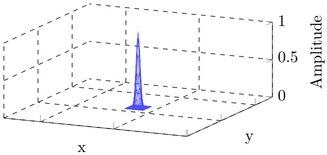

Arbitrary numerical acquisition s_2

- **5 sources**,
- **80**m **depth**,
- **multi-point sources**,

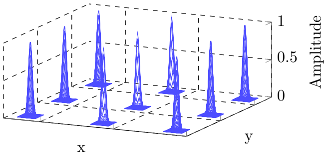

- No need to known observational source wavelet.
- Differentiation impossible with least squares types misfit.

Experiment with different obs. and sim. acquisition

Data from frequency between 3 to 15 Hz, domain size $2.5 \times 1.5 \times 1.2$ km, **Simulation using 5 sources only**.

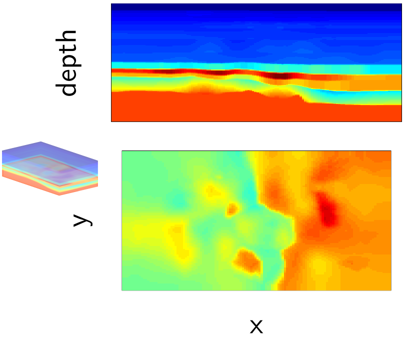

(a) True velocity

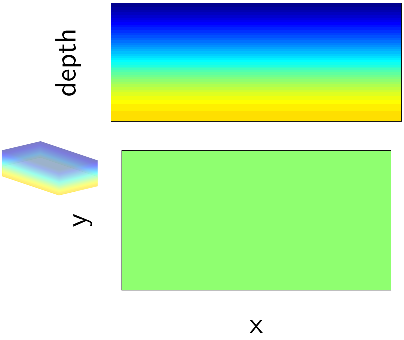

(b) Starting velocity

Experiment with different obs. and sim. acquisition

Frequency from 3 to 15 Hz, $2.5 \times 1.5 \times 1.2$ km,
Simulation using 5 **sources only**. **-33%** computational time.

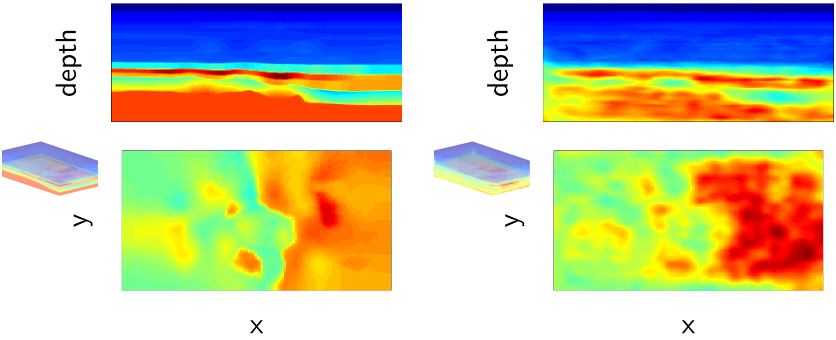

(a) True velocity (b) 15 Hz reconstruction

Plan

Conclusion

Seismic inverse problem using pressure and vertical velocity data:

- appropriate cost function to minimize,
- allow minimal information on the acquisition setup,
- other applications,
- perspective: design the most efficient numerical setup,
- Rk: possible for elastic media with measures of traction.

Conclusion

Seismic inverse problem using pressure and vertical velocity data:

- appropriate cost function to minimize,
- allow minimal information on the acquisition setup,
- other applications,
- perspective: design the most efficient numerical setup,
- Rk: possible for elastic media with measures of traction.

Quantitative reconstruction algorithm toolbox for time-harmonic wave,

- Discontinuous Galerkin discretization in HPC framework,
- large scale optimization scheme using back-scattered data,
- acoustic, elastic, anisotropy, 2D, 3D, attenuation.

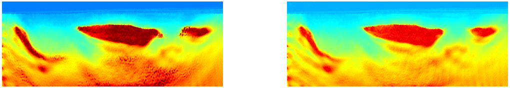

P- and S-wavespeed reconstructions

Conclusion

Seismic inverse problem using pressure and vertical velocity data:

- appropriate cost function to minimize,
- allow minimal information on the acquisition setup,
- other applications,
- perspective: design the most efficient numerical setup,
- Rk: possible for elastic media with measures of traction.

Quantitative reconstruction algorithm toolbox for time-harmonic wave,

- Discontinuous Galerkin discretization in HPC framework,
- large scale optimization scheme using back-scattered data,
- acoustic, elastic, anisotropy, 2D, 3D, attenuation.

THANK YOU

Appendix

Stability of the Helmholtz Inverse Problem

$$\|c_1^{-2} - c_2^{-2}\| \leq \mathcal{C}\left(\|F(c_1^{-2}) - F(c_2^{-2})\|\right)$$

G. Alessandrini
Stable determination of conductivity by boundary measurement
Applicable Analysis 1988

N. Mandache
Exponential instability in an inverse problem for Schrödinger equation
Inverse Problems 2001

Stability of the Helmholtz Inverse Problem

$$\|c_1^{-2} - c_2^{-2}\| \leq \mathcal{C}\left(\overbrace{\|F(c_1^{-2}) - F(c_2^{-2})\|}^{\delta}\right)$$

- c_1^{-2}: target
- c_2^{-2}: initial model
- $F(c_1^{-2})$: observation
- $F(c_2^{-2})$: simulation

- Stability associate data and model correspondence
- Reconstruction is based on the iterative minimization of the difference between observation and simulation using an initial model.

G. Alessandrini
Stable determination of conductivity by boundary measurement
Applicable Analysis 1988

N. Mandache
Exponential instability in an inverse problem for Schrödinger equation
Inverse Problems 2001

Stability of the Helmholtz Inverse Problem

$$\|c_1^{-2} - c_2^{-2}\| \leq \mathcal{C}\Big(\overbrace{\|F(c_1^{-2}) - F(c_2^{-2})\|}^{\delta}\Big)$$

target (c_1^{-2}), initial model (c_2^{-2}), observation ($F(c_1^{-2})$), simulation ($F(c_2^{-2})$)

- Stability associate data and model correspondence
- $\mathcal{C}(\delta) \leq C\Big(\log(1+\delta^{-1})\Big)^{-\alpha}$

G. Alessandrini
Stable determination of conductivity by boundary measurement
Applicable Analysis 1988

N. Mandache
Exponential instability in an inverse problem for Schrödinger equation
Inverse Problems 2001

Conditional Lipschitz stability: assumptions

- $c(x)$ is bounded $B_1 \leq c^{-2}(x) \leq B_2$ in Ω
- $c(x)$ has a piecewise constant representation of size N

$$c(x)^{-2} = \sum_{k=1}^{N} c_k \chi_k(x)$$

- Ω has Lipschitz boundary

$$\|c_1^{-2} - c_2^{-2}\|_{L^2(\Omega)} \leq \mathcal{C} \, \|F(c_1^{-2}) - F(c_2^{-2})\| \qquad (1)$$

G. Alessandrini and S. Vessella
Lipschitz stability for the inverse conductivity problem
Advances in Applied Mathematics 2005

E. Beretta, M. V. de Hoop, F. and O. Scherzer
Inverse boundary value problem for the Helmholtz equation: quantitative conditional Lipschitz stability estimates.
SIAM Journal of Mathematical Analysis 2016

Formulation

The stability constant is bounded

$$\frac{1}{4\omega^2} e^{K_1 N^{1/5}} \leq \mathcal{C} \leq \frac{1}{\omega^2} e^{(K(1+\omega^2 B_2) N^{4/7})} \qquad (2)$$

- depends on the partitioning N and the frequency ω

E. Beretta, M. V. de Hoop, F. and O. Scherzer
Inverse boundary value problem for the Helmholtz equation: quantitative conditional Lipschitz stability estimates 2016

Conditional Lipschitz stability for Cauchy data

In the case of partial Cauchy data (p and $\partial_\nu p$), we have that, we can obtain a Lipschitz type stability:

$$\|c_1^{-2} - c_2^{-2}\| \leq \mathcal{C}\big(\mathcal{J}_{\mathcal{G}}(c_1^{-2}, c_2^{-2})\big)^{1/2}$$

Where c_1^{-2} and c_2^{-2} are piecewise linear.